Q. J. R. Meteorol. Soc. (2006), **132**, pp. 1073–1089 doi: 10.1256/qj.04.108

Formation and release of symmetric instability following Delta-M adjustment

By C. J. MORCRETTE* and K. A. BROWNING
Department of Meteorology, University of Reading, UK

(Received 16 July 2004; revised 13 January 2006)

SUMMARY

Conditional Symmetric Instability (CSI) and Delta-M adjustment have both been suggested as possible mechanisms to explain the slantwise circulations that lead to two-dimensional precipitation bands near midlatitude cold fronts. Previous work has shown how the initial state required for CSI to occur is similar to the state produced as a result of Delta-M adjustment. An idealized dry numerical model is used to test the hypothesis that slantwise circulations can occur due to the release of symmetric instability formed by the Delta-M adjustment process. The numerical simulation shows the coexistence of two pairs of slantwise circulations: one due directly to Delta-M adjustment, and the other which occurs in a region of symmetric instability which was formed by the Delta-M adjustment process. The simulated circulation is qualitatively similar to some high-resolution Doppler radar observations of vertically stacked slantwise circulations. It is argued that a combined Delta-M/CSI mechanism may also be responsible for the creation of multiple slantwise circulations in the moist atmosphere.

KEYWORDS: Cross-frontal circulations Slantwise convection

1. INTRODUCTION

Observations have shown that multiple bands of precipitation sometimes form in the horizontal plane close to midlatitude cold fronts (Hobbs 1978). These multiple precipitation bands imply a complex circulation in the cross-frontal plane. Indeed, observations have been made of multiple vertically stacked slantwise circulations occurring across a cold front (Browning *et al.* 2001).

Two mechanisms, Conditional Symmetric Instability (CSI; Bennetts and Hoskins 1979) and Delta-M (ΔM, the absolute momentum anomaly) adjustment (Holt and Thorpe 1991), have been discussed in the literature to explain the formation of shallow-slope circulations, or slantwise convection in the near-two-dimensional (2D) environment close to an ana-cold front. These slantwise circulations can create regions of conditional instability at mid-levels, leading to near-2D narrow bands of precipitation. The slantwise circulations resulting from these two mechanisms are similar, both having updraughts aligned along isentropic surfaces. Additionally, once circulations due to the release of CSI or due to ΔM adjustment have decayed, the atmosphere is left is a state which will be close to conditional symmetric neutrality (Fischer and Lalaurette 1995b) and no observation of the atmosphere will make it possible to determine retrospectively which mechanism has occurred. Similarly, Thorpe and Emanuel (1985) have shown how weak frontogenesis, occurring in an atmosphere with small conditional symmetric stability, leads to circulations which, if they were observed, would make it difficult to decide whether they were due to either frontogenesis or CSI. Consequently, when looking at observations of slantwise circulations, it is important to realise that frontogenesis, conditional symmetric instability *and* ΔM adjustment may have contributed to the characteristics of the circulations.

Bennetts and Hoskins (1979) state that the initial state required for the release of CSI to occur corresponds to the presence of a saturated region of negative moist potential vorticity (PV). Holt and Thorpe (1991) and Fischer and Lalaurette (1995b) showed how the final state obtained after ΔM adjustment has occurred contains

* Corresponding author: Department of Meteorology, University of Reading, Earley Gate, PO Box 243, Reading RG6 6BB, UK. e-mail: c.j.morcrette@reading.ac.uk

© Royal Meteorological Society, 2006.

a region of negative PV. The fact that these two states are similar has not been commented upon or been investigated.

Schultz and Schumacher (1999) suggest, however, that areas susceptible to CSI may occur close to areas susceptible to gravitational convection. The convection occurring in such areas could then exhibit characteristics of gravitational convection, slantwise convection or a combination of both, with the possibility of evolution from one type to another. This concept of convective-symmetric instability, one that Schultz and Schumacher (1999) state requires further investigation, will be investigated in this paper.

We propose the hypothesis that ΔM adjustment and the release of CSI could occur together, and suggest how circulations due to such a combined mechanism would be different from the circulations that would be observed if only one of the mechanisms had operated. Using a new dry idealized numerical model, we then show that ΔM adjustment can create a region of dry symmetric instability and that this instability is then released. It is argued that the coexistence in the dry simulation of slantwise updraughts due to ΔM adjustment, and of slantwise updraughts occurring in a region of dry symmetric instability, indicates that the possibility of both moist ΔM adjustment and CSI occurring concurrently should be considered when analysing observations of vertically stacked slantwise circulations or multiple bands of precipitation.

2. A HYPOTHESIS LINKING LINE CONVECTION, ΔM ADJUSTMENT AND CSI

It is tantalizing to note how the initial state required for CSI to occur, i.e. a region of negative moist PV, corresponds to the final state obtained following ΔM adjustment in a moist atmosphere. Consequently, we ask whether the two mechanisms of ΔM adjustment and CSI could occur consecutively, as cause and effect, the slantwise circulation due to ΔM adjustment creating a region where CSI can be, and is, released leading to the formation of further slantwise circulations. The coexistence of ΔM adjustment and CSI is hinted at in the literature (e.g. Browning *et al.* 2001), but as far as the authors know, no explicit linking mechanism has been proposed and no such interaction has yet been simulated.

Figure 1 illustrates a thought experiment, describing a hypothetical series of events, which would allow ΔM adjustment and CSI to occur consecutively. This hypothetical life-cycle is described graphically using a series of sketches, most of which are inspired by the numerical simulations of Holt and Thorpe (1991), Fischer and Lalaurette (1995a,b) and Thorpe and Rotunno (1989). Striving for clarity, these sketches try to capture the important features of their numerical simulations by subjectively smoothing their results and by removing some of the confusing noise. Each of the panels of Fig. 1 is now described in turn.

(*a*) *Initial conditions and line convection*

The sketches represent a vertical (x, z) cross-section through a baroclinic zone, with the cross-section aligned perpendicular to the thermal wind, with colder air on the left and warmer air on the right (Fig. 1(a)). The along-front wind flows into the plane of the diagram and increases with height. These sketches represent a region around 5 km deep and a few hundreds of kilometres wide. The shaded regions show where the saturated equivalent PV (EPV) is negative and hence where moist gravitational, inertial or moist symmetric instabilities are present (Schultz and Schumacher 1999; Schultz *et al.* 2000). The EPV is defined as $= (1/\rho)\ \zeta \cdot \nabla\theta_e^*$, where ρ is the density, ζ is the absolute vorticity and θ_e^* is the saturated equivalent potential temperature. In a well-mixed convective boundary layer, there will be a uniform distribution of

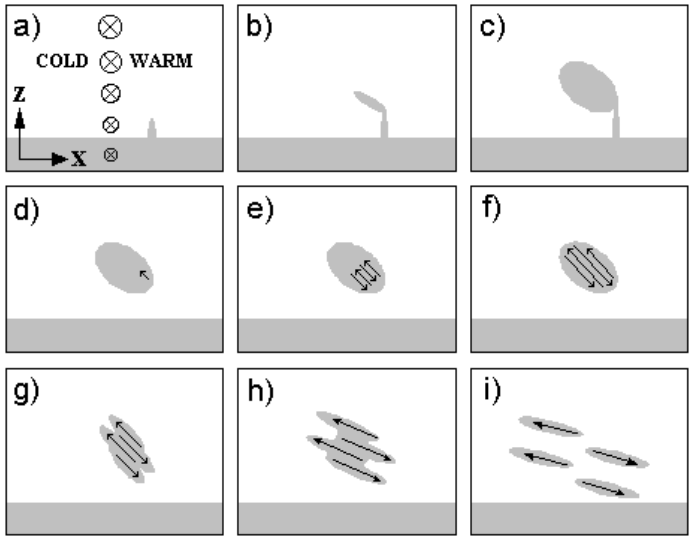

Figure 1. A thought experiment linking line convection, ΔM adjustment and CSI in the development of slantwise convection. These sketches show a time series (a)–(i) of vertical cross-sections through a baroclinic zone, normal to the thermal wind. The vertical cross-sections represent an area around 5 km deep and several hundreds of kilometres wide. Areas of negative equivalent potential vorticity are shaded. The first, second and third row of panels represent three distinct stages which are dominated by ΔM adjustment, linear CSI and non-linear CSI respectively. Further details are given in the text in section 2.

equivalent potential temperature, θ_e, with height. If the boundary layer is horizontally homogeneous, then the EPV will be zero. However, a small amount of vertical shear of the horizontal wind and a small horizontal temperature gradient will be sufficient to make the EPV in the boundary layer negative. Above the boundary layer, in the free troposphere, potential temperature tends to increase vertically, while the vertical moisture gradients are quite small, so the EPV is positive. Line convection due to forced ascent at an ana-cold front advects negative EPV out of the boundary layer and into the free troposphere and creates a negative EPV 'chimney' (Fischer and Lalaurette 1995b).

(*b*) ΔM *adjustment*

The parcels in the line convection will rise vertically, until they reach their level of neutral buoyancy. As the parcels ascend, they conserve their moist potential temperature and geostrophic absolute momentum (Eliassen 1962; Lilly 1986). However, since the atmosphere is baroclinic, the geostrophic absolute momentum at the level of neutral buoyancy is different from that at a parcel's initial height, so an absolute momentum anomaly, ΔM, has been generated. The parcels then experience an inertial acceleration which force them towards a region whose ambiant geostrophic absolute momentum is the same as the parcels'. This inertial adjustment occurs along a neutral buoyancy surface which, since the atmosphere is baroclinic and the isentropic surfaces are not horizontal, has a small component in the vertical direction, so the parcels will move along a shallow slantwise path. This mechanism is known as 'ΔM adjustment' (Holt and Thorpe 1991; Fischer and Lalaurette 1995b). After having ascended vertically, parcels from the boundary layer will move towards the cold side of the line convection (Fig. 1(b)), creating a negative EPV lens or bulge on the cold side of the negative EPV 'chimney'. CSI does not yet start being released at this stage, as the unstable region is

too small and because it is of the wrong aspect ratio to allow CSI circulations to form within it.

(*c*) *Formation of a region of negative EPV*

Holt and Thorpe (1991) showed that a region of negative *dry* PV was formed as a result of a *dry* ΔM adjustment process, while if moisture is included, Fischer and Lalaurette (1995b) showed that ΔM adjustment leads to the formation of a region of negative *equivalent* PV (Fig. 1(c)). This region of negative EPV can be thought of as having been advected from the boundary layer. We will now assume, for the purpose of this thought experiment, that the line convection then ceases, although this does not necessarily occur in nature.

(*d*) *CSI triggered in negative EPV region formed by* ΔM *adjustment*

In inviscid CSI theory, the fastest-growing mode has updraughts of vanishingly small width (Xu 1986). When viscosity is taken into account, the updraughts are still narrow, but they now have a finite width. Consequently regions of negative EPV can actually be stable to viscous CSI depending on their geometry (Thorpe and Rotunno 1989). Assuming that the whole of the negative-EPV region created by the ΔM adjustment is saturated, and that, as the region grows, the geometry is now such that it is unstable to viscous CSI, then only a triggering mechanism is needed for the CSI to be released. Here we hypothesize that the remains of the ΔM-adjustment circulation, the updraught of which is aligned along θ_e surfaces, could provide the perturbation oriented within the 'wedge of instability', that is in a direction between the saturated equivalent potential temperature, θ_e^*, and geostrophic absolute momentum, M_g, isopleths, and hence in the right direction to trigger the CSI (Fig. 1(d)).

(*e*) *Linear CSI*

While the circulation occupies only a small portion of the unstable region (Fig. 1(e)), the circulation is in its *linear* phase and grows exponentially, in a manner consistent with the predictions made by *linear* instability theory using the *linearized* equations of motion (Bennetts and Hoskins 1979; Fischer and Lalaurette 1995a).

(*f*) *Growth of circulation within negative EPV region*

As the circulation grows to fill the negative EPV region (Fig. 1(f)), the circulations themselves begin to change the background state in which they are embedded. Consequently linear CSI theory, which assumes a static background state, can no longer accurately describe the evolution of the circulation, which now evolves in a highly nonlinear manner and has entered its mature phase (Fischer and Lalaurette 1995a).

(*g*) *Nonlinear CSI; circulations distort the negative EPV region*

During the mature stage, as the circulations modify the background, they are changing it towards a state of symmetric neutrality and hence removing the instability. As the atmosphere becomes less unstable, the growth rate decreases and the perturbation kinetic energy will soon reach its peak, before starting to decay (Fischer and Lalaurette 1995a, Fig. 12). Once the circulation fills the entire region of negative EPV, negative EPV will begin to be advected out of the region which initially had negative values into areas which were initially positive, and vice versa. This distorts the shape of the negative EPV region (as shown in Fig. 1(g) and also in Fischer and Lalaurette (1995a)).

(*h*) *Slope of circulations becomes shallower*

In the symmetrically unstable region, the isentropes are steeper than the absolute momentum isopleths. Symmetric instability can be thought of as a convective instability along an absolute momentum surface. When the symmetric instability is released, the isentropes become shallower, while the absolute momentum isopleths become steeper. When the isentropes and absolute momentum isopleths are parallel, the atmosphere is symmetrically neutral, indicating that the instability has been released. As the background state is stabilized, and the isentropic surfaces become shallower, the slantwise updraughts, which are aligned along them, also become shallower (as shown in Fig. 1(h) and also in Fischer and Lalaurette (1995a)). As the atmosphere approaches stability, the growth rate decreases further and the circulations will enter their decay stage.

(*i*) *EPV region breaks up*

If there are several circulations present, one below the other, then a large region of negative EPV can get broken up, or sheared out, into smaller patches of negative EPV (Fig. 1(i)). For a given eddy viscosity, the patches of negative EPV, which would be unstable if the fluid were inviscid, become stable at a certain height-to-width aspect ratio (Emanuel 1979; Thorpe and Rotunno 1989). It is interesting to speculate about what would happen if the remnants of a CSI circulation were to reach the top of the boundary layer and perturb it (Morcrette 2004). It may be that some potentially unstable parcels at the top of the boundary layer would get lifted to saturation making them free to convect. This convection would be likely to occur in a location different from the original line convection. As the environment is still baroclinic, the new convection will still generate an absolute momentum anomaly and ΔM adjustment will follow. In principle, the whole cycle could repeat itself several times.

To summarize, line convection in a baroclinic atmosphere will lead to ΔM adjustment and the formation of a region of negative moist PV at mid-levels. We hypothesize that once this region is large enough to enable CSI circulations to form within it, and if this negative moist PV region were to be saturated, then the motion due to ΔM adjustment may trigger the instability, allowing CSI to be released. The coexistence of slantwise circulations due to ΔM adjustment and the release of CSI will create a complex cross-frontal flow, which cannot then be explained as being due to only one of the mechanisms. This combined mechanism could explain multiple circulations in the vicinity of frontal line convection, while ordinary ΔM adjustment would be able to explain the presence of only a single updraught. Additionally, by allowing the ΔM-adjustment circulation to predispose the atmosphere for CSI, this mechanism could explain multiple circulations appearing in regions where no saturated region of negative EPV was previously present. The possibility of ΔM adjustment creating a region of symmetric instability and this instability then being released, forming further slantwise circulations, will now be investigated using a new idealized numerical model.

3. Description of the numerical model

Different numerical models could be used to perform these experiments, such as a numerical weather-prediction model, or a large-eddy model. Both types of model include sophisticated dynamics, and a large number of parametrizations to represent different physical processes. Here we adopted the ethos of using the simplest possible tool. Rather than using a simplified version of a very complex numerical model, we set out to build the most simple numerical model that would serve our purpose.

A new idealized numerical model has been designed. The circulation in the plane of interest can be described using one component of the vorticity equation. Variations along the direction of the front are neglected, so the model becomes two dimensional.

Latent heat release is almost certainly going to contribute to the development of the slantwise circulations described in the previous section. However, we argue that the *essence* of the mechanism under investigation is an interaction between the gravitational and inertial forces active in ΔM adjustment and symmetric instability, and that the effects of moisture are not of primary importance. Consequently, we assume that the flow is dry adiabatic, as well as frictionless, allowing a simple thermodynamic equation to be used. Using a dry numerical model also ensures that the humidity distribution does not become the limiting factor preventing the hypothesized interaction from taking place.

This new model, which has been specifically designed to *M*odel the *I*nteraction between *D*elta-M *A*djustment and *S*ymmetric instability, has been named MIDAS. It represents a vertical slice taken perpendicular to a baroclinic zone and will be used to simulate the circulation in the cross-frontal plane due to the two mechanisms, ΔM adjustment and dry symmetric instability.

(*a*) *Derivation of dynamical equations*

Following convention, the coordinate axes are taken such that x is the across-front direction, y is the along-front direction, and z is the vertical direction. We also define u, v and w as the velocity components in the x, y and z directions, respectively. This allows the Boussinesq form of the momentum equations (White 2002) to be written as:

$$\frac{\mathrm{D}u}{\mathrm{D}t} = fv - \frac{\partial \phi'}{\partial x} \tag{1}$$

$$\frac{\mathrm{D}v}{\mathrm{D}t} = -fu - \frac{\partial \phi'}{\partial y} \tag{2}$$

$$\frac{\mathrm{D}w}{\mathrm{D}t} = \frac{g}{\theta_0}\theta' - \frac{\partial \phi'}{\partial z}, \tag{3}$$

where $\mathrm{D}/\mathrm{D}t = \partial/\partial t + \mathbf{u}\cdot\nabla$ is the Lagrangian derivative, $\mathbf{u}$ is the three-dimensional velocity vector, f is the Coriolis parameter, $\phi' = p'/\rho$ is a normalized pressure perturbation, g is the acceleration due to gravity, θ_0 is a constant reference value of potential temperature and θ' is a perturbation potential temperature. By differentiating Eq. (3) with respect to x and taking it away from Eq. (1) differentiated with respect to z, we obtain

$$\frac{\mathrm{D}\eta}{\mathrm{D}t} = f\frac{\partial v}{\partial z} - \frac{g}{\theta_0}\frac{\partial \theta}{\partial x}, \tag{4}$$

where $\eta = (\partial u/\partial z) - (\partial w/\partial x)$ is the component of vorticity in the y direction, and the ϕ terms have cancelled each other out. The y component of vorticity describes the circulation in the cross-frontal plane. This equation shows that departures from thermal wind balance drive the circulation in the cross-frontal plane.

In this model we assume that the front is 2D, so only a 2D slice perpendicular to the front needs to be considered. Some 3D aspects are retained by including an along-front wind, v, which represents flow in and out of the x, z plane. As we assume that there are no variations along the length of the front, then $\partial\phi'/\partial y = 0$, and Eq. (2) can be written as

$$\frac{\mathrm{D}v}{\mathrm{D}t} = -fu. \tag{5}$$

Our equation set is completed by using a form of the thermodynamic equation. Dry adiabatic frictionless flow is assumed, so potential temperature is conserved following air parcels, and hence

$$\frac{\mathrm{D}\theta}{\mathrm{D}t} = 0. \tag{6}$$

By expanding out the Lagrangian derivative, Eqs. (4), (5) and (6) can be written in the form in which they will be solved by the numerical model:

$$\frac{\partial \eta}{\partial t} = J(\psi, \eta) + f\frac{\partial v}{\partial z} - \frac{g}{\theta_0}\frac{\partial \theta}{\partial x} + \Delta(\eta) \tag{7}$$

$$\frac{\partial v}{\partial t} = J(\psi, v) - fu + \Delta(v') \tag{8}$$

$$\frac{\partial \theta}{\partial t} = J(\psi, \theta) + \Delta(\theta'). \tag{9}$$

The advection terms have been written in terms of a Jacobian, $J(\,.\,,.)$, and diffusion terms, $\Delta(.)$, have been added for numerical stability. The stream function, ψ, is defined such that $u = \partial\psi/\partial z$ and $w = -\partial\psi/\partial x$.

(*b*) *Numerical methods*

All derivatives are found by using finite-difference schemes which are accurate to second order. An Arakawa Jacobian is used to calculate the advection term as it conserves mean kinetic energy, mean vorticity and mean enstrophy over the domain (Haltiner and Williams 1980). The diffusion terms are made up of horizontal and vertical parts, each of which consists of the second derivative of the field to be diffused:

$$\Delta(\varphi) = \nu_\mathrm{h}\frac{\partial^2\varphi}{\partial x^2} + \nu_\mathrm{v}\frac{\partial^2\varphi}{\partial x^2}, \tag{10}$$

where φ is η, v' or θ' in Eqs. (7, 8 and 9). The values of diffusivity for the three fields of vorticity, perturbation potential temperature and perturbation along-front wind were found experimentally, by searching for values that prevent the appearance of grid-scale noise in the respective field, without leading to too much diffusion. The horizontal diffusivities for the three fields are the same, with a value of $\nu_\mathrm{h} = 1 \times 10^4\ \mathrm{m^2 s^{-1}}$. The vertical diffusivities, ν_v, are a factor $(\mathrm{d}x/\mathrm{d}z)^2$ smaller than the horizontal ones, so that two-grid-length waves are damped at the same rate in the two directions.

As the model integrates vorticity forward in time, then at each time step the stream function, which is required for use in the advection scheme, must be calculated from the vorticity at the previous time step. The Poisson equation, $\eta = \nabla^2\psi$, is solved for ψ, by using 2D fast Fourier transforms. Periodic boundary conditions are used on the lateral boundaries and free-slip conditions are used at the top and bottom rigid boundaries.

The first time step is calculated using a forward-difference scheme and all subsequent time steps are found using a centred-difference scheme. A Robert–Asselin time filter is used to dampen the effects of the computational mode, and to couple the two solutions arising from using a centred-in-time, centred-in-space scheme (Haltiner and Williams 1980).

The vertical grid spacing is 20 m, so that features with scales of 150–200 m can be resolved, allowing the model simulations to be compared to observations made by the Chilbolton Doppler radar. The aspect ratio of vertical to horizontal grid length was chosen to be 1:100 to ensure that very shallow circulations could be resolved

(Persson and Warner 1991), leading to a horizontal grid spacing of 2 km. The time step is 4 seconds.

The model has a rigid lid at a height of 20.48 km. A damping layer is introduced by adding a Newtonian relaxation term to the three prognostic variables, following the method described by Shutts and Gray (1994), but with the damping coefficient $\gamma_0 = 5 \times 10^{-5}$ s^{-1} at a starting height of 12 km and with a damping height-scale of 2.5 km. The model domain was 4096 km wide. Experiments were carried out with a domain of twice the width. These confirmed that the periodic boundary conditions did not have a significant affect on the circulations of interest.

4. Experimental set-up

The initial conditions for this simulation consist of a dry statically stable troposphere, with $N^2 = (g/\theta_0)\partial\theta/\partial z = 10^{-4}$ s^{-2}, above a 1 km deep neutral boundary layer. There is a tropopause at 10 km, above which the static stability rises to 5×10^4 s^{-2}. The changes in static stability, at the top of the boundary layer and at the tropopause, are defined using half a cosine wave, and ensure a smooth transition over 300 m and 2 km, respectively. The stream function is initially zero everywhere, so the the cross-frontal and vertical components of the flow are zero at the start of the simulation. The along-front wind is zero at the surface and is defined aloft by setting $S^2(x, z) = (g/\theta_0)\partial\theta/\partial x = f\partial v/\partial z = S_0^2 \sin(2\pi x/L)$, where L is the width of the domain. A value of $S_0^2 = 5 \times 10^{-7}$ s^{-2} was used in the troposphere, corresponding to a vertical shear of the along-front wind of 5 m s^{-1}km^{-1}. Above 10 km, S_0^2 is reduced smoothly to zero, over a height of 4 km. This avoids unrealistically strong wind speeds near the top of the model, which could lead to inertial instability. The initial state is defined to be in thermal-wind balance so this distribution of along-front wind implies the presence of a broad frontal zone, which together create a baroclinic region in the troposphere where the absolute momentum isopleths are not vertical, allowing large absolute momentum anomalies to be generated when upright convection takes place. The initial distributions of potential temperature and along-front wind over the entire domain are shown in Fig. 2. Due to the need to have periodic boundary conditions, a warm front is present as well as a cold front and two jets are present within the domain.

Once the simulation starts, heating is applied over a region 16 km wide and 160 m deep near the surface (i.e. 8 grid points wide and 8 grid points high) in the region of strongest baroclinicity. This heating will lead to a narrow region of upright convection and is intended to represent the forced ascent ahead of an ana-cold front. The heating is increased smoothly, over a period of 30 minutes, eventually leading to that area having a 6 K temperature anomaly. Experiments were carried out heating the surface for varying amounts of time. If the heating is only applied for a few hours, a small absolute momentum anomaly is created above the surface, and a ΔM-adjustment circulation forms, but without any region of symmetric instability forming. If the heating is applied for more than around 12 hours, the first ΔM adjustment circulation has had time to develop and lead to slantwise circulations aloft while surface heating, generating further momentum anomalies, is still occurring. This leads to complicated circulations, where multiple ΔM-adjustment circulations occur, and dominate over any circulation occurring within the symmetrically unstable regions. Heating for 8 hours was found to be optimal, and results from that simulation will be discussed in detail. Simulations with surface heating applied for 6, 7, 9 and 10 hours were qualitatively very similar. In each case the heating is reduced to zero over a period of 30 minutes rather than being switched off abruptly. The circulations are then allowed to evolve freely for the

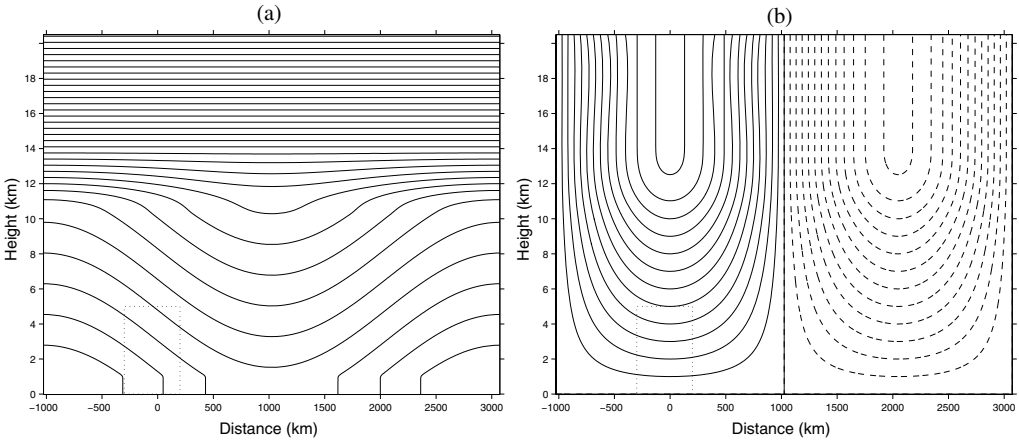

Figure 2. The initial distributions of (a) potential temperature (contour interval 5 K) and (b) along-front wind (contour interval 5 m s^{-1}), with positive flow into (negative flow out of) the page shown by solid (dashed) contours. The entire model domain is shown, while the sub-region shown in the results section is indicated by dotted lines.

remainder of the 33-hour simulation. Simulations were also carried out using larger horizontal grid lengths, such as 4 and 8 km. These coarser simulations also produced similar circulations, although the surface heating had to be applied for longer before comparable regions of inertial instability, leading to ΔM adjustment, were formed. Once the heating was switched off, the coarser simulations also took longer to evolve.

Each of the evolving circulations was compared to Doppler radar observations and examined for consistency with the hypothesized sequence of events described in section 2.

5. Results

Multiple regions of slantwise ascent developed during the numerical simulation. The structure of these simulated circulations closely resembles the structure of the multiple-stacked slantwise circulations observed using Doppler radar by Browning *et al.* (2001). Figure 3 shows a comparison between the system-relative cross-frontal velocities observed using the Chilbolton Doppler radar (51.145°N, 1.437°W) on 10 February 2000 and the cross-frontal velocities in one of the simulations performed by the numerical model. The similarities are encouraging. Both circulations show a narrow region of upright convection ascending 2 km and then feeding a region of shallow slope, or slantwise, convection. A second region of slantwise ascent is visible below the main updraught. Regions of descending motion can be seen interspersed between the regions of shallow slope ascent.

Having shown that the numerical model is able to produce multiple slantwise circulations which are very similar to observed structures, the evolution of the simulation with 2 km horizontal grid length will now be described in detail. This will be done by considering different variables in turn: potential temperature, absolute momentum and PV, and then cross-frontal horizontal and vertical velocities.

(*a*) *Potential temperature, absolute momentum and potential vorticity*

The evolution of the potential temperature and absolute momentum fields is shown in Fig. 4. Initially, we see a baroclinic atmosphere with a neutral boundary layer (Fig. 4(a)). After 3 hours, low values of absolute momentum have been advected out

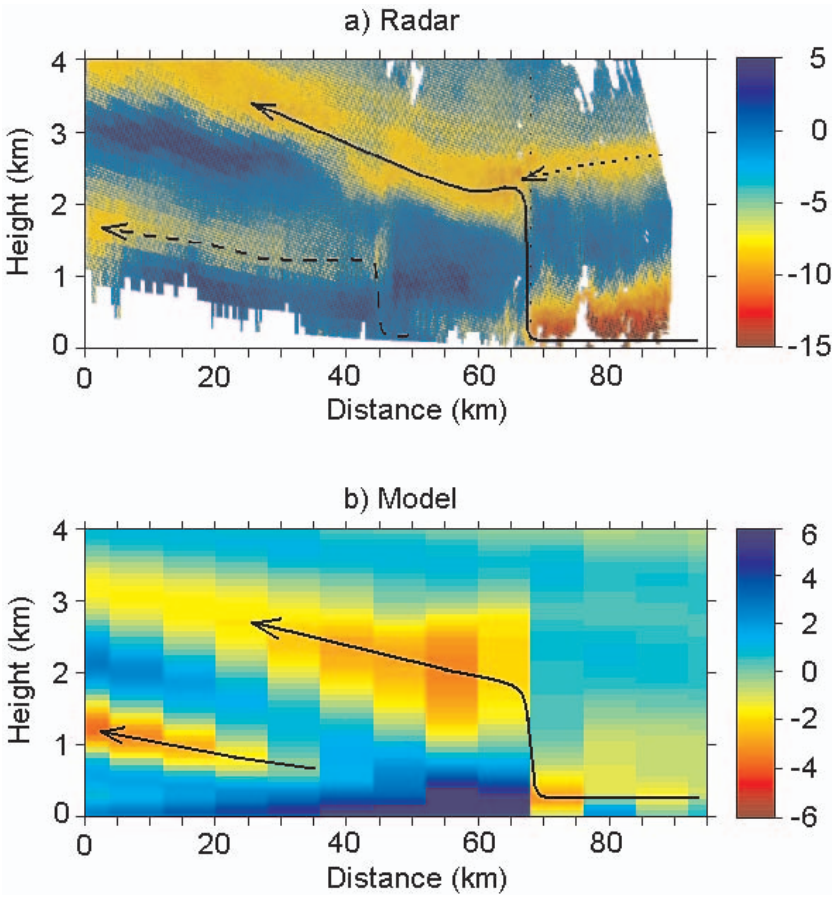

Figure 3. (a) Doppler radar observations of system-relative cross-frontal wind component (m s^{-1}). The observations were made on 10 February 2000, using the 3 GHz Chilbolton radar and are adapted from Browning *et al.* (2001). (b) Numerical simulation of horizontal cross-frontal flow (m s^{-1}). Localized surface heating in a baroclinic atmosphere leads to line convection, ΔM adjustment and the generation of a region of symmetric instability. The release of the symmetric instability forms a second region of rearward-sloping slantwise ascent. This image was taken from a simulation with 8 km horizontal grid length, after 60 hours of surface heating.

of the boundary layer by the line convection resulting from the surface heating, leading to a buckled M surface and the generation of an inertial instability (Fig. 4(b)). As the inertial instability is released by the ΔM-adjustment process, the position of the buckle on the M surface moves up the isentropic surface (Fig. 4(c)).

The evolution of the negative PV during the simulation is shown in Fig. 5. Initially all the negative PV is confined within the boundary layer (Fig. 5(a)). Localized heating near the surface leads to upright convection, and to negative PV being advected out of the boundary layer (Fig. 5(b)). As ΔM adjustment takes place, some of the negative PV which has been advected up to the mid-levels gets advected quasi-horizontally towards the cold side of the front (Fig. 5(c)).

After 6 hours (Fig. 4(c)), a region of symmetric instability has formed aloft on the cold side of the main updraught. This region of dry symmetric instability has been formed by the circulation due to forced line convection and ΔM adjustment. However, the release of the inertial instability present at the top of the updraught

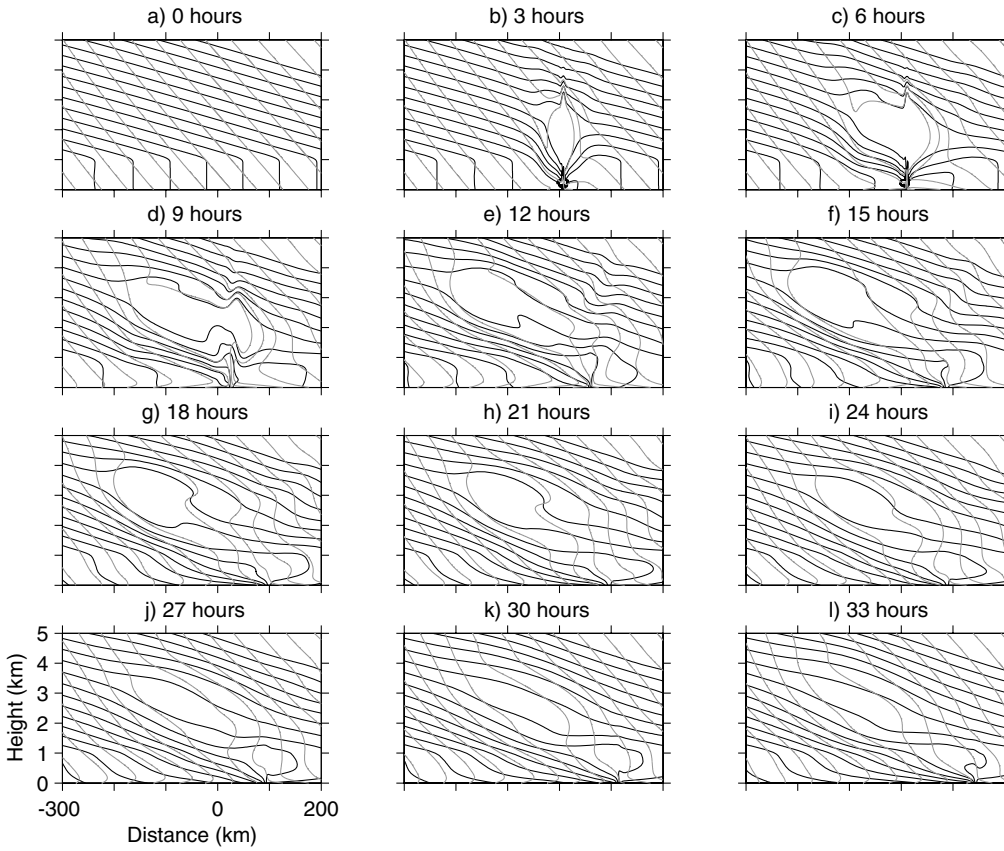

Figure 4. The evolution at 3-hourly intervals of the potential temperature (black contours with interval 1 K) and absolute momentum per unit mass (grey contours with interval 5 m s^{-1}). The scale is 500 km in the horizontal and 5 km in the vertical.

will dominate over any circulations due to the symmetric instability. By 9 hours into the simulation (Fig. 4(d)), the advection of parcels by the ΔM-adjustment process, conserving M and θ, has forced the M and θ surfaces apart on the cold side of the vertical updraught. Since the vertical potential temperature and horizontal absolute momentum gradients have been reduced, the PV in this region will be low or even negative (Figs. 5(d) and (e)). After 15 hours, the area where the M and θ lines have been forced apart has moved upwards and to the cold side of where it was after 6 hours. The symmetric instability identified in Fig. 4(c) has been partially released, with some of the M and θ surfaces now parallel, showing that the atmosphere is now symmetrically neutral in that region (Fig. 4(e)). As the circulation continues to evolve, the dry convective and inertial instabilities created as a result of the surface heating are being released (Figs. 4(g) and 5(g)), such that by 21 hours into the simulation *a region of dry symmetric instability has formed, where the isentropes are steeper than the absolute momentum contours* (Figs. 4(h) and 5(h)). After 24 hours, there are no convective or inertial instabilities remaining aloft, only regions of dry symmetric instability (Figs. 4(i) and 5(i)). As negative PV is advected out of the boundary layer into the free troposphere, positive PV is advected down from the free troposphere, making the boundary layer behind the cold front convectively stable, and preventing upright convection from occurring there. The region of dry symmetric instability reduces in size over the next

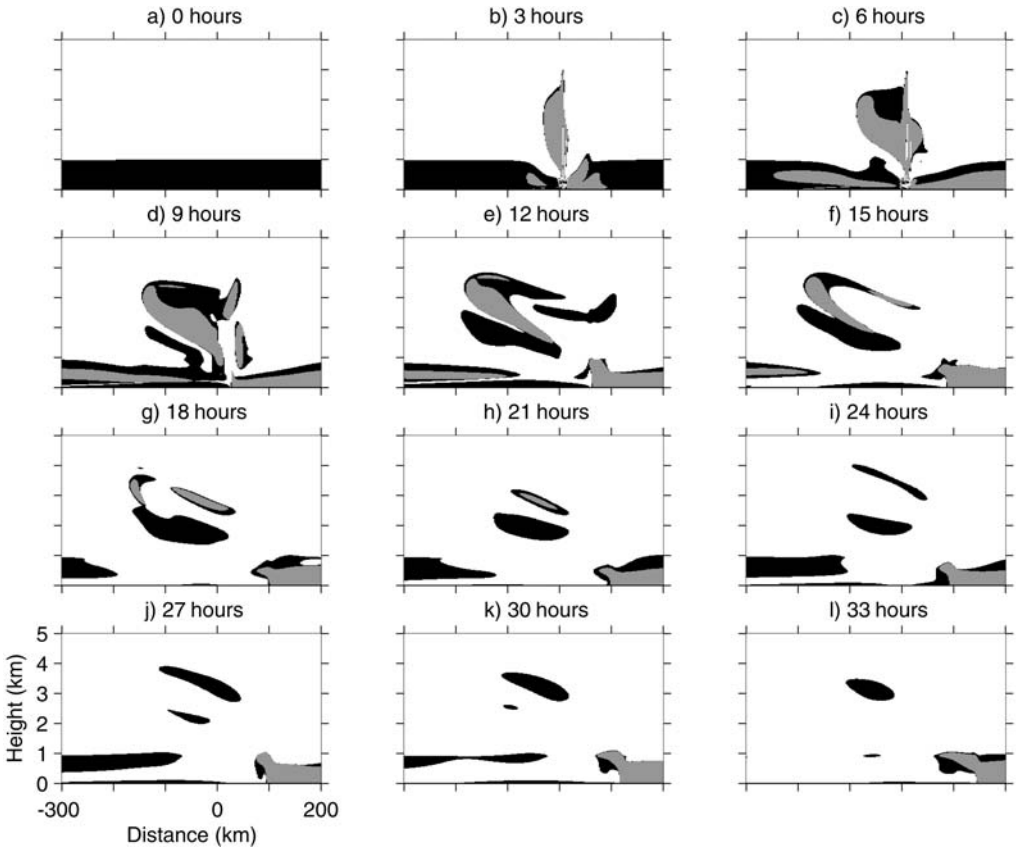

Figure 5. The distribution of negative potential vorticity derived from the numerical simulation at 3-hourly intervals. The grey shaded regions indicate negative PV due to convective or inertial instabilities, while the black shading shows where the PV is negative due to the presence of dry symmetric instability. (Positive PV is shown as white.) The horizontal scale is 500 km and the vertical scale is from the surface to 5 km. This figure should be compared to the hypothesized evolution shown in Fig. 1.

few hours (Figs. 5(j)–(l)) as the potential temperature and absolute momentum contours relax back towards their initial positions (Figs. 4(j)–(l)). Having described the evolution of the potential temperature, absolute momentum and PV fields, we can now look at the velocities associated with these circulations.

(*b*) *Horizontal cross-frontal and vertical velocities*

The horizontal cross-frontal and vertical velocities associated with the circulations in the simulation are shown in Figs. 6 and 7, respectively. The flow is initially at rest (Figs. 6(a) and 7(a)). For the first few hours after the heating is switched on (Figs. 6(b) and 7(b)), the circulation looks very similar to what would be expected during upright convection in a barotropic environment, i.e. there is convergence at low levels and divergence at the top of the updraught, with weak subsidence around the updraught. By 6 hours into the simulation, baroclinic effects have broken the symmetry of the circulation with the strongest horizontal velocities and a well-defined region of rearward-sloping ascent occurring on the cold side of the vertical updraught (Figs. 6(c) and 7(c)). From 15 hours into the simulation, a second slantwise updraught can be

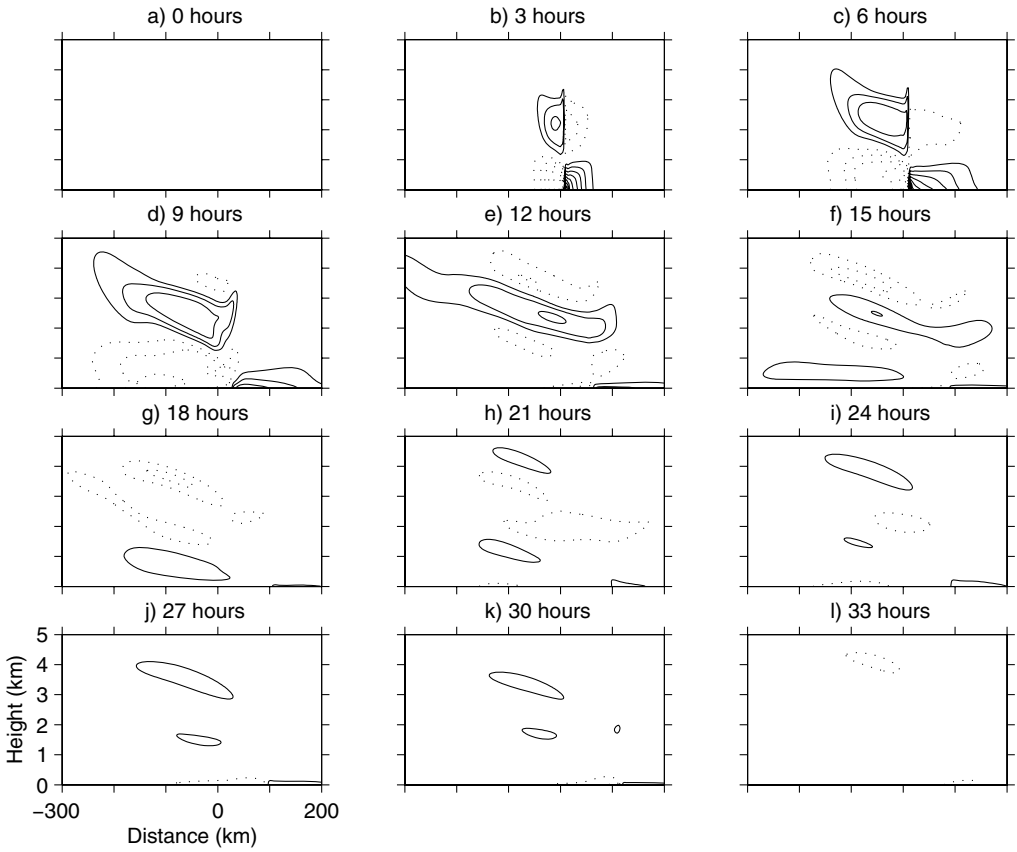

Figure 6. The horizontal cross-frontal velocity in the simulation at 3-hourly intervals out to 33 hours. The contour interval is 2 m s^{-1}, with dotted (solid) contours indicating flow from left to right (right to left). The zero contour is not shown. The scale is 500 km in the horizontal and 5 km in the vertical.

seen below the main ΔM-adjustment updraught (Figs. 6(f) and 7(f)). The appearance of a second region of slantwise ascent during a ΔM-adjustment mechanism was not observed by either Holt and Thorpe (1991) or Fischer and Lalaurette (1995b) and is a new feature of this simulation. This second region of rearward-sloping ascent reaches a peak vertical velocity of 2 cm s^{-1} after 21 hours (Fig. 7(h)) and has a horizontal velocity of 2 m s^{-1} rearward with respect to the system (Fig. 6(h)).

(*c*) *Stream function*

Figure 8 confirms that non-zero stream function only reaches halfway across the domain after around 24 hours. Experiments carried out with a domain of twice the width were subjectively indistinguishable within the small region of interest shown in Figs. 4, 5, 6 and 7. Figure 8 also shows that perturbations to the stream function are being damped as they pass through the stratosphere and that no reflections are occurring off the rigid lid at the top of the model.

6. Discussion

The slantwise circulations described in section 5 have been simulated using a numerical model that neglects the effects of moisture. However, when multiple slantwise

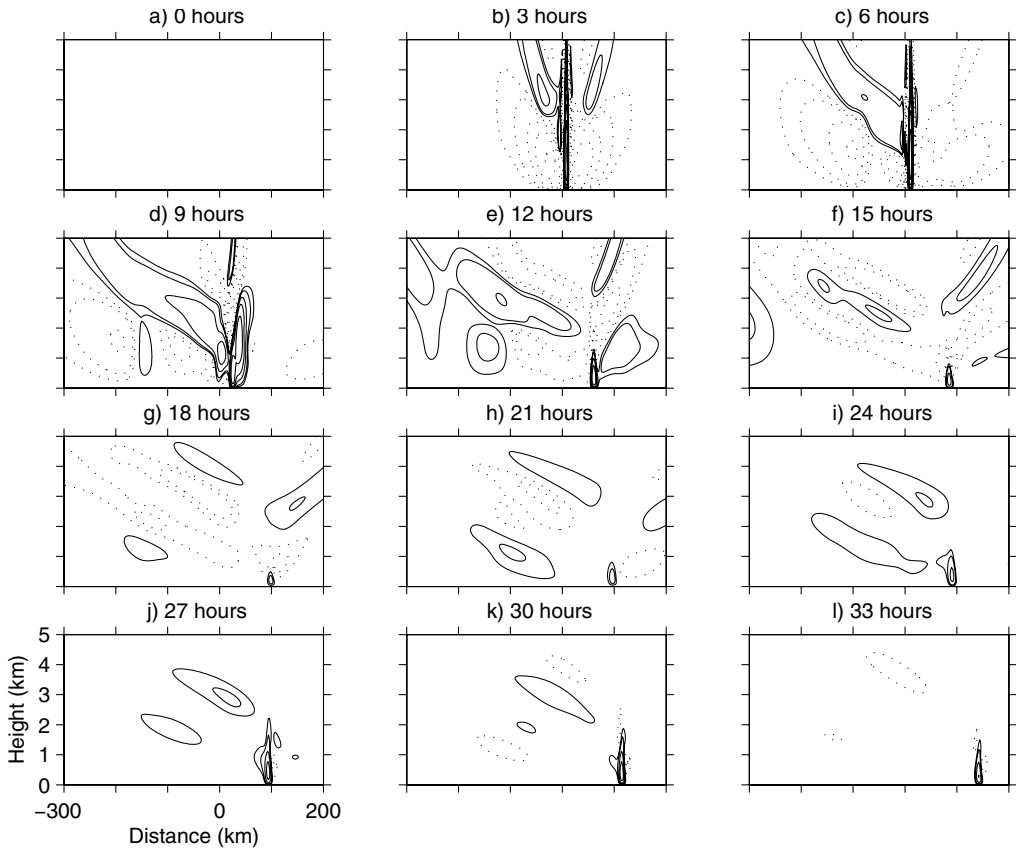

Figure 7. The vertical velocity in the simulation at 3-hourly intervals out to 33 hours. Contours are drawn at ±0.01, 0.02, 0.05, 0.1, 0.2, 0.5, 1, 2 and 5 m s^{-1}, with the solid (dotted) contours representing ascent (descent). The scale is 500 km in the horizontal and 5 km in the vertical.

circulations are observed, it is generally in frontal regions where latent heat release due to phase changes in water substance have almost certainly played a role in the evolution of the flow. Indeed, the mere detection of a Doppler signal at 3 GHz, as shown in Fig. 3(a), implies the presence of precipitation within the frontal region, and suggests condensation heating in the updraughts and evaporative cooling in the downdraughts below them.

However, we argue that the key point in the hypothesized interaction between ΔM adjustment and CSI, discussed in section 2, is actually an interaction between the gravitational and inertial forces, and that the effects of latent heating are of secondary importance. Indeed, the identification of symmetric instability, or inertial instability along an isentropic surface, as one of the possible instabilities of an axisymmetric baroclinic vortex by Solberg (1936), was done using a dry framework. Similarly, Holt and Thorpe's (1991) idea of the release of convective instability in a baroclinic atmosphere generating an inertial instability and then leading to a slantwise circulation was also developed using a dry model. Both of these concepts have since been developed by including the effects of moisture (e.g. Bennetts and Hoskins (1979) and Fischer and Lalaurette (1995b)); however, the underlying mechanisms can be understood by neglecting the effects of moisture. Consequently, we believe that the results of the dry

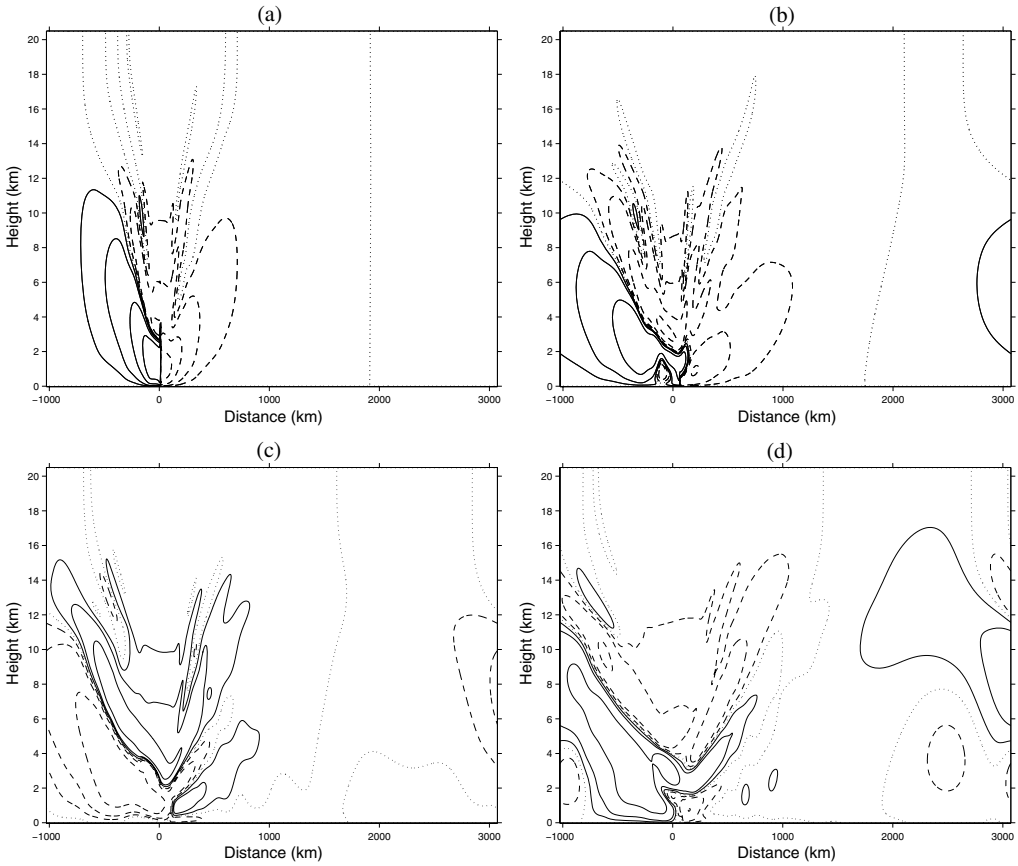

Figure 8. The stream function over the whole model domain after: (a) 6, (b) 12, (c) 18 and (d) 24 hours. Contours are drawn at 0 and ±100, 300, 1000, 3000 and 10000, with positive (negative) contours solid (dashed) and the zero contour dotted.

simulation can provide insight into the qualitative nature of the circulations occurring in the real atmosphere. The inclusion of latent heat due to condensation in the updraughts and sublimation in the downdraughts in models of frontogenesis showed that the circulations intensified (Sawyer 1956; Parker and Thorpe 1995). If the effects of latent heat release were to be included in our simulation, it would be reasonable to expect that the strength of the circulations would increase and, consequently, modelled circulations such as that shown in Fig. 3(b) would be more quantitatively comparable with the observed velocities shown in Fig. 3(a).

In section 2, we hypothesized that CSI could form in the negative EPV region formed by ΔM adjustment and presented a series of idealized sketches to show how the PV might evolve under such conditions. In the interest of clarity, in the idealized sketches presented in Fig. 1 the negative PV region formed by ΔM adjustment was not allowed to start releasing its symmetric instability until *after* the upright convection feeding the ΔM adjustment had stopped. This is reasonable as the negative PV region needs to be of a certain size before symmetric instability circulations are able to form within it. In the hypothesis presented in Fig. 1, the line convection was switched off just as the negative PV region reached such a size. If this were to occur in the simulation or in reality, it would be easy to separate the circulations into the part due to ΔM adjustment

and the part due to the release of the CSI. In the simulation, however, the symmetric instability starts being removed soon after it is formed. This early on, it is probably circulations due to the upright convection and ΔM adjustment that effectively remove the instability, rather than the instability being released as such. Either way, regions of symmetric instability as deep and wide as those depicted in Fig. 1 are never seen in the simulation, but they do exist. This appears to be in agreement with Emanuel's (1988) hypothesis that slantwise convective adjustment occurs on time-scales which are shorter than those of the processes that create the instability, hence explaining that conditions of moist symmetric neutrality, rather than moist symmetric instability, are often observed. It is also possible that no large regions of symmetric instability are created because an instability can only accumulate if there is something inhibiting its release. In this case, as the symmetric instability is forming in the vicinity of ascent regions due to ΔM adjustment, then those updraughts are providing the trigger necessary for the release of the instability.

It could be argued that this simulation is just showing the ΔM-adjustment process leading to the formation of a region of symmetric neutrality. However, we have shown that small regions of symmetric instability were formed below the ΔM-adjustment updraught, and that a second updraught formed in the region where this instability was being released. The formation of this second updraught cannot be explained by the ΔM-adjustment process as described by Holt and Thorpe (1991) or Fischer and Lalaurette (1995b). A complex cross-frontal circulation, with multiple regions of slantwise ascent as observed by Browning *et al.* (2001), can be created only if the circulations due to both the following processes persist for long enough to coexist over some period of time: (a) the initial ΔM adjustment, and (b) the subsequent release of symmetric instability created by the ΔM-adjustment process.

7. Conclusion

The mechanisms of ΔM adjustment and CSI both lead to slantwise circulations with updraughts aligned nearly along the isentropes. As a result, Fischer and Lalaurette (1995b) note that once the circulations have reached their mature stage, it will be very difficult, when looking at observations, to distinguish which of the mechanisms was responsible for the slantwise circulation.

Since CSI theory can easily explain the formation of periodic circulations, by the growth of the most unstable normal mode (Fischer and Lalaurette 1995a,b), it is tempting when looking at observations of multiple circulations to assume that they must be due only to the release of CSI. Similarly, if the observations suggest that strong line convection was occurring at the cold front, it can be wrongly concluded that the circulation is due only to the ΔM-adjustment mechanism.

The simulation presented here shows that it is possible for the two mechanisms of ΔM adjustment and dry symmetric instability to *coexist*, each of them leading to the formation of a slantwise circulation and thereby resulting in multiple stacked circulations. The possibility of ΔM adjustment and conditional symmetric instability both occurring in the same cold front must therefore be considered when trying to understand some of the observed multiple slantwise circulations in the atmosphere.

Acknowledgements

This work constitutes part of the PhD thesis of the lead author. Financial assistance was provided by the Natural Environment Research Council and was supplemented by

a CASE award from the Met Office. The lead author would like to thank Dr Glenn Shutts, who was a joint supervisor on this project, for the many helpful theoretical discussions. Thanks are also due to Dr Suzanne Gray for her encouragement and advice.

REFERENCES

Bennetts, D. A. and Hoskins, B. J. 1979 Conditional symmetric instability—a possible explanation for frontal rainbands. *Q. J. R. Meteorol. Soc.*, **105,** 945–962

Browning, K. A., Chapman, D. and Dixon, R. S. 2001 Stacked slantwise convective circulations. *Q. J. R. Meteorol. Soc.*, **127,** 2513–2536

Eliassen, A. 1962 On the vertical circulation in frontal zones. *Geofys. Publ.*, **24,** 147–160

Emanuel, K. A. 1979 Inertial instability and mesoscale convective systems. Part I: Linear theory of inertial instability in rotating viscous fluids. *J. Atmos. Sci.*, **36,** 2425–2449

1988 Observational evidence of slantwise convective adjustment. *Mon. Weather Rev.*, **116,** 1805–1816

Fischer, C. and Lalaurette, F. 1995a Meso-β-scale circulations in realistic fronts. I: Steady basic state *Q. J. R. Meteorol. Soc.*, **121,** 1255–1283

1995b Meso-β-scale circulations in realistic fronts. II: Frontogenetically forced basic states. *Q. J. R. Meteorol. Soc.*, **121,** 1285–1321

Haltiner, G. J. and Williams, R. T. 1980 *Numerical prediction and dynamic meteorology.* John Wiley and Sons, 2nd edition

Hobbs, P. V. 1978 Organisation and structure of clouds and precipitation on the mesoscale and microscale in cyclonic storms. *Rev. Geophys. Space Phys.*, **16,** 741–755

Holt, M. W. and Thorpe, A. J. 1991 Localized forcing of slantwise motion at fronts. *Q. J. R. Meteorol. Soc.*, **117,** 943–963

Lilly, D. K. 1986 Instabilities. Chapter 11 in *Mesoscale meteorology and forecasting*, Ed. P. S. Ray, American Meteorol. Soc.

Morcrette, C. J. 2004 'Radar and modelling studies of upright and slantwise convection'. PhD thesis, Department of Meteorology, University of Reading, UK

Parker, D. J. and Thorpe, A. J. 1995 The role of snow sublimation in frontogenesis. *Q. J. R. Meteorol. Soc.*, **121,** 763–782

Persson, P. O. G. and Warner, T. T. 1991 Model generation of spurious gravity waves due to inconsistency of vertical and horizontal resolution. *Mon. Weather Rev.*, **119,** 917–935

Sawyer, J. S. 1956 The vertical circulation at meteorological fronts and its relation to frontogenesis. *Proc. R. Soc. London*, 346–362

Schultz, D. M. and Schumacher, P. N. 1999 The use and misuse of conditional symmetric instability. *Mon. Weather Rev.*, **127,** 2709–2732

Schultz, D. M., Schumacher, P. N. and Doswell III, C. A. 2000 The intricacies of instabilities. *Mon. Weather Rev.*, **128,** 4143–4148

Shutts, G. J. and Gray, M. E. B. 1994 A numerical modelling study of the geostrophic adjustment process following deep convection. *Q. J. R. Meteorol. Soc.*, **120,** 1145–1178

Solberg, H. 1936 Le mouvement d'inertie de l'atmosphère stable et son role dans la théorie des cyclones. *Proces-Verbaux des séances de l'Union International de Géodésie et Géophysique (IUGG)*, Edinburgh, **2,** 66–82

Thorpe, A. J. and Emanuel, K. A. 1985 Frontogenesis in the presence of small stability to slantwise convection. *J. Atmos. Sci.*, **42,** 1809–1824

Thorpe, A. J. and Rotunno, R. 1989 Nonlinear aspects of symmetric instability. *J. Atmos. Sci.*, **46,** 1285–1299

White, A. A. 2002 A view of the equations of meteorological dynamics and various approximations. Pp. 1–100 in *Large-scale atmosphere–ocean dynamics*, **I,** Eds. J. Norbury and I. Roulstone, Cambridge University Press

Xu, Q. 1986 Conditional symmetric instability and mesoscale rainbands. *Q. J. R. Meteorol. Soc.*, **112,** 315–334